Aberrations and retinal image quality of the normal human eye

Junzhong Liang and David R. Williams

Center for Visual Science, University of Rochester, Rochester, New York 14627

Received January 7, 1997; revised manuscript received May 12, 1997; accepted May 20, 1997

We have constructed a wave-front sensor to measure the irregular as well as the classical aberrations of the eye, providing a more complete description of the eye's aberrations than has previously been possible. We show that the wave-front sensor provides repeatable and accurate measurements of the eye's wave aberration. The modulation transfer function of the eye computed from the wave-front sensor is in fair, though not complete, agreement with that obtained under similar conditions on the same observers by use of the double-pass and the interferometric techniques. Irregular aberrations, i.e., those beyond defocus, astigmatism, coma, and spherical aberration, do not have a large effect on retinal image quality in normal eyes when the pupil is small (3 mm). However, they play a substantial role when the pupil is large (7.3-mm), reducing visual performance and the resolution of images of the living retina. Although the pattern of aberrations varies from subject to subject, aberrations, including irregular ones, are correlated in left and right eyes of the same subject, indicating that they are not random defects. © 1997 Optical Society of America [S0740-3232(97)00811-9]

1. INTRODUCTION

The most important optical instrument is the human eye, yet its optical performance has not been completely characterized. In addition to exhibiting some defocus and astigmatism, normal eyes are known to suffer from spherical aberration[1,2] and comalike aberrations.[3,4] On the basis of subjective observations of the retinal image of point sources, Helmholtz emphasized the existence of additional ocular aberrations that are not found in conventional, man-made optical systems.[5] In concordance with Helmholtz's view, measurements of the eye's wave aberration[6–8] suggest that the eye has irregular aberrations that correspond to more abrupt, local variations in phase error. However, we have no quantitative information about these aberrations or their importance for vision and imaging the retina.

Liang *et al.*[9] recently demonstrated a new technique to measure the eye's wave aberration, based on the Hartmann–Shack principle.[10] To provide a more complete description of all the aberrations of the eye, we have improved the wave-front sensor by increasing the density of samples taken of the wave-front slope in the pupil. Moreover, we use a description of each eye's wave aberration that includes up to tenth-order aberrations, corresponding to 65 aberrations, or Zernike modes. In the first part of this paper we examine the repeatability and accuracy of aberration measurements obtained with the new wave-front sensor. We then compare the modulation transfer function of the eye with a 3-mm pupil computed from the wave aberration with that obtained under similar conditions on the same observers with the double-pass and interferometric techniques. We find that the wave aberration measured with the wave-front sensor accounts for most of the loss in modulation transfer measured with the other techniques. We also find that aberrations greater than fourth order do not seriously degrade image quality in normal eyes when the pupil is small. However, such higher-order aberrations have a significant effect on retinal image quality for the dilated pupil and can influence visual performance as well as the resolution of images of the retina.

2. METHOD

A. Illumination Path

Figure 1 shows the apparatus. Planes conjugate with the retina are labeled "r," and those conjugate with the eye's pupil are labeled "p." Linearly polarized light from a He–Ne laser (632.8 nm, 5 mW) passed through an acousto-optic modulator that controlled the exposure duration on the observer's retina. The acousto-optic modulator had an extinction ratio of 10^{-4}, which allowed enough light through when the beam was nominally off to provide the observer with a fixation target. The beam then passed through neutral density filters followed by a spatial filter. The spatial filter consisted of a 40× microscope objective that focused the beam onto a 25-μm pinhole. The emerging beam was collimated by lens L_1. After reflection from a mirror, the beam was reflected by a polarizing beam splitter toward the eye. Lens L_2 formed an image of the pinhole that was conjugate with the retina. The point source subtended 0.31′ of arc at the retina. For all measurements the total light energy entering the eye was less than 3 μJ, which is approximately 200 times less than the American National Standards Institute's maximum permissible exposure.[11]

B. Imaging Path

On the return path, only the depolarized light from the retina was transmitted by the polarization beam splitter. The beam splitter rejected the highly polarized light reflected by lenses as well as the first Purkinje image from the cornea. Lenses L_3, L_2, L_4, and L_5 imaged the subject's pupil onto a hexagonal array of lenslets. Each

0740-3232/97/112873-11$10.00

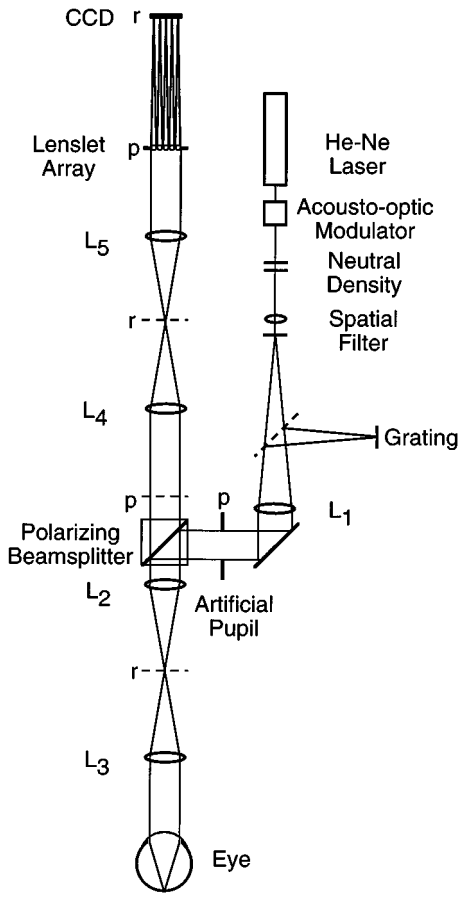

Fig. 1. Hartmann–Shack wave-front sensor for the eye. Light from a He–Ne laser produces a compact point source on the retina. If the eye has aberrations, the wave front of the light returning from the retina forms a distorted wave front at the pupil plane. This wave front is recreated by lenses L_3, L_2, L_4 and L_5 at the plane of lenslet array. The two-dimensional lenslet array samples this warped wave front and forms an array of focused spots on a CCD array. Each of the spots from the lenslets is displaced on the CCD array in proportion to the slope of the wave front; the wave aberration itself can be calculated from this displacement.

lenslet had an aperture of 0.5 mm and a focal length of 97 mm. The wave aberration was measured across either a 3.4-mm pupil or a 7.3-mm pupil. For the 3.4-mm pupil measurements, the pupil was magnified 2.5 times, so that the pupil was sampled with a center-to-center spacing of 0.2 mm. For the 7.3-mm pupil measurements, lens L_5 was changed so that the pupil was magnified 1.17 times, and the center-to-center spacing in the pupil was 0.43 mm. Each lenslet forms an aerial image of the retinal point source on a cooled, scientific-grade CCD camera. The wave-front sensor measures an aberrated wave front emerging from the eye in reference to a perfect plane wave at the eye's entrance pupil. This is equivalent to measuring the wave-front error of the eye at the exit pupil in reference to a perfect reference sphere.[9]

C. Measurements with Small Pupils

Two sets of measurements of the wave aberration were made with 3.4-mm pupils. The first set was made on the eyes of three subjects whose modulation transfer functions (MTF's) were measured before with the double-pass and interferometric techniques.[12] The second set was made on nine other eyes with a slightly different procedure.

For comparison with double-pass and interferometric MTF's, measurements were made on the right eyes of RNB, DRW, and DHB, whose ages were 36, 40, and 34, respectively. These observers were mildly myopic [0.2, 1.6, and 0.4 diopters (D), respectively]. In addition, DRW had 0.8 D of astigmatism. In measuring these three eyes we used the same alignment procedure as in the earlier study.[12] Accommodation was paralyzed with two drops of cyclopentolate hydrochloride (1%). During the alignment procedure before the measurements, the observer adjusted the horizontal and vertical positions of his eye to optimize the image quality of an 18-c/deg horizontal square-wave grating. We chose this criterion for alignment because the goal of the earlier study was to measure the best image quality possible in the human eye. A mirror temporarily placed between the spatial filter pinhole and lens L_1 allowed the observer to view the grating, which was sandwiched against a diffuser and was backlit with 630-nm light. The grating lay at the same optical distance as the pinhole from the eye. Lens L_3 was attached to the bite-bar mount so that the observer could focus the grating by translating his eye together with the lens along the optical axis. Corrective lenses were not worn during the experiment. The entrance pupil for the beam was 3 mm and was determined by an artificial pupil in the back focal plane of L_2. The observer's head was stabilized with a bite bar.

For each observer, 20 images were obtained, each corresponding to an exposure of 2 s on the retina. The use of this long exposure reduced the speckle in the images, because eye movements cause slightly different retinal regions to be illuminated by the point source over time, which alters the speckle pattern. This has the effect of improving signal-to-noise ratio. Nonetheless, we found similar results with the shortest exposures that we tried, which were 100 ms. All images were obtained in a single experimental session.

The measurements made for 3.4-mm pupils on nine other observers used a similar procedure, except for the following. Each eye was aligned, not for optimum image quality as before, but with respect to the center of the natural pupil. For these measurements no drug was used to dilate the pupil. At the beginning of the measurement on each eye, the subject adjusted his horizontal position until the left side of the pupil occluded his view of the point source he was fixating. He repeated this task using the right side, the top, and the lower margin of the pupil. The average of two settings in each of these four locations was taken as the center of the entrance pupil. This served as the origin of the coordinate system in which the wave aberration was defined. The standard deviation for the center of the entrance pupil with this alignment technique was less than 0.1 mm. We reduced the eye's defocus by asking the observer to translate his eye together with the lens (L_3) along the optical axis to optimize image quality of the point source. The diameter of the laser beam at the entrance pupil was 1.5 mm in-

stead of 3 mm. Subject age ranged from 21 to 38. All had normal visual acuity and required a correction for defocus and astigmatism of less than 3 D.

D. Measurements with Large Pupils

Using the same procedures used on the nine observers described above, we made measurements on 14 eyes (nine observers) for a 7.3-mm pupil. The pupil was dilated with tropicamide (1%). The exposure duration was 1 s. Three images, taken within 60 s, were averaged. Subject age ranged from 21 to 38. All had normal visual acuity and had less than 3 D of defocus and astigmatism.

3. RESULTS

A. Wave Aberration of the Eye

Figure 2 shows results for the 3.4-mm pupil. Figure 2a. shows the expected result if an eye with perfect optics had been used. It was obtained by introducing a plane wave into the imaging path at the point where the eye's pupil would normally have been. The image consists of a highly regular array of spots, one spot for each lenslet of the wave-front sensor. Figures 2b. and 2c. show the images obtained from real eyes. Aberrations in real eyes displaced each spot relative to the corresponding spot in the reference image obtained with a planar wave front. The displacement is proportional to the local slope of the wave front at that lenslet. The local wave-front slope in the x and y directions was measured at 217 locations simultaneously across the pupil. The wave aberration was computed from the array of local slopes with a least-squares technique.[9,13] We represented the wave aberration with the sum of 65 Zernike polynomials, corresponding to aberrations up to and including tenth order.[14] Figures 2e. and 2f. show contour plots of the reconstructed wave aberration for each observer, averaged across 20 exposures. The wave aberration shown has been truncated to a pupil diameter of 3 mm. The spacing between contour lines is 0.15 μm, which is roughly $\lambda/4$ at 632.8 nm.

Figures 3a.–c. show the images obtained with the large (7.3-mm) pupil from three real eyes. Figures 3d.–f. show the contour plots of the wave aberration for three of the observers with the 7.3-mm pupil. The raw images as well as the reconstructed wave aberration from real eyes reveal substantial local, irregular aberrations that are not evident with the smaller pupil. For example, subject ML has an arc-shaped ridge on the upper third of the plot that corresponds to the location where his eyelid normally rests against the cornea.

Observer JL was atypical in that he showed a substantial amount of spherical aberration. The spherical aberration in his eye, like that in almost all eyes that had any appreciable spherical aberration, was in the direction that the rays entering the margin of the pupil experienced higher power than those entering near the center. All the eyes revealed less spherical aberration than would be expected from a simplified eye with a single spherical refracting surface. Approximately 1/3 of the eyes showed almost no spherical aberration.

B. Repeatability of the Wave-Aberration Measurements

Figure 4a. shows with square symbols a vertical cross section through the wave aberration for one observer, RNB, measured with the small (3.4-mm) pupil. The error bars represent ± 1 standard deviation based on the 20 exposures taken within a single session. The standard deviation averages ~ 0.046 μm or $\sim \lambda/14$ ($\lambda = 0.633$ μm), indicating that the wave-aberration measurements are highly repeatable. The wave aberration obtained when a plane wave passing through a 0.5-D trial lens replaced

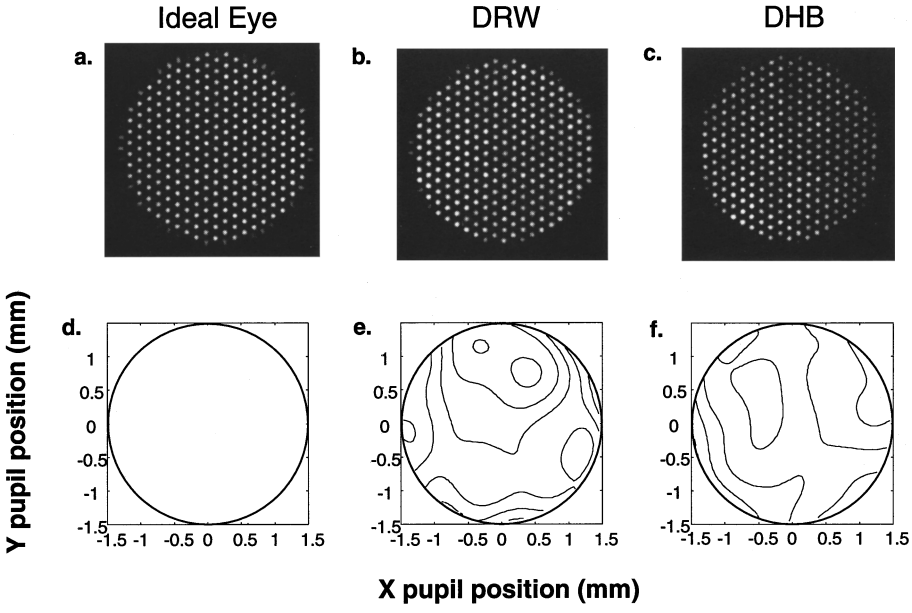

Fig. 2. Wave-front-sensor images and wave aberration of eyes for a small 3-mm pupil. a. The image from the wave-front sensor for an ideal eye on the left, which corresponds to no phase error across the pupil, as shown in the wave aberration on the right. b. and c. show the wave-front-sensor images for two real eyes along with the calculated wave aberration. The contour interval in the wave-aberration plots (d.–f.) is 0.15 μm. The pupil was sampled with a center-to-center spacing of 0.2 mm.

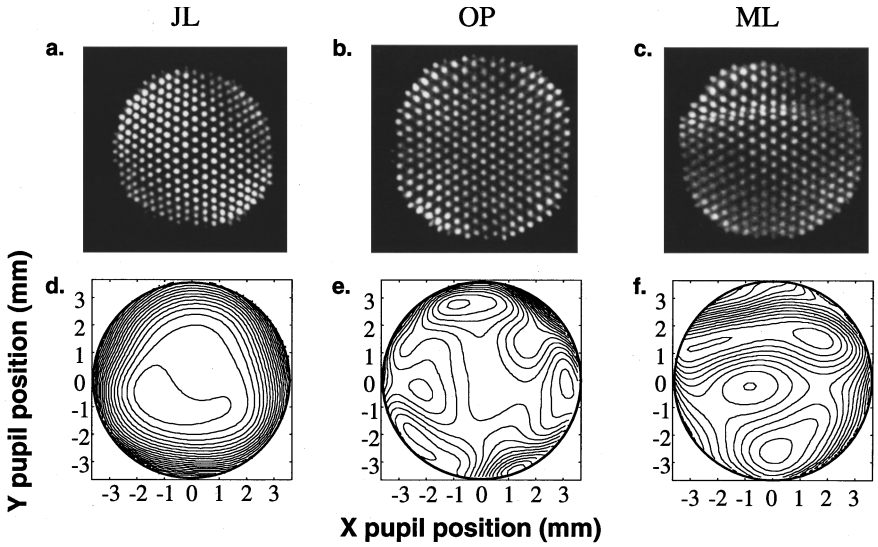

Fig. 3. Wave-front-sensor images and wave aberration of eyes for a 7.3-mm pupil. a.–c. are the wave-front-sensor images for three observers. The center-to-center spacing of lenslets in the pupil was 0.42 mm. d.–f. are the corresponding wave aberrations of the three eyes from measurements of the wave-front slopes. The contour interval in the wave-aberration plots is 0.15 μm for OP and 0.3 μm for JL and ML. Defocus and astigmatism have been removed from the wave aberrations, thus showing the presence of substantial irregular aberrations. The peak-to-valley wave-front error for the 7.3-mm pupil is approximately 7 μm, 4 μm, and 5 μm for JL, OP, and ML, respectively.

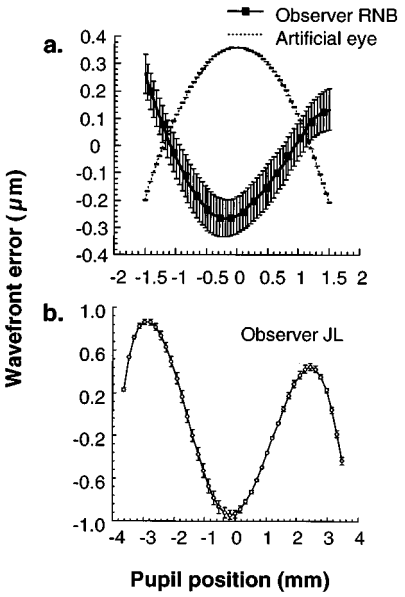

Fig. 4. Repeatability of measurements with the wave-front sensor. a. Measurements of the wave aberration along one cross section of a 3-mm pupil for a real eye (RNB) and an artificial eye. b. Measurement of the wave aberration along one cross section of a 7.3-mm pupil for observer JL. The error bars are ±1 standard deviation.

the light that would exit the eye's pupil is shown with the dashed curve in Fig. 4. The mean of the standard deviation of these measurements is only 0.0013 μm or ~λ/487, 35 times smaller than the standard deviation when a real eye was measured. This shows that the variability due to the instrument is considerably smaller than that introduced by the eye. Possible sources of variability include fluctuations in focus and possibly other aberrations (despite the use of cyclopentolate hydrochloride), small movements of the eye and head, and variations in the thickness of the tear film. Eye movements probably have a very small effect on the wave-front measurement, because the shift of pupil position is small for the fixating eye. For example, a relatively large fixational eye movement of 10 arc min produces a pupillary displacement of less than 35 μm, which is a small fraction of the spacing between samples taken in the pupil. Our results with the wave-front sensor show that the important aberrations correspond to gradual enough variations in phase across the pupil that normal fixational eye movements are not a problem. In addition, the images acquired by the CCD camera with real eyes contain some laser speckle that is not present when a plane wave is introduced into the system. Laser speckle, which changes from exposure to exposure, adds variability to the measurements.

Figure 4b. shows with circular symbols a vertical cross section through the wave aberration for one of the observers (JL) measured for a large (7.3-mm) pupil. The standard deviation averages ~0.052 μm or ~λ/12, again showing the high repeatability of the wave-front measurement for the large (7.3-mm) pupil.

C. Accuracy of the Wave-Front Sensor

We assessed the accuracy with which the wave-front sensor can measure known aberrations by introducing defocus of known amounts into the system. We passed a plane wave through a spherical trial lens positioned where the eye's pupil would otherwise have been and then into the wave-front sensor. The measured dioptric power of the trial lens was calculated from the corresponding mode of the Zernike expansion of the wave aberration.

Figure 5 shows the relationship between the measured power and the nominal dioptric power of the trial lens over an 8-D range. The discrepancy between the nominal and the measured power never exceeded 0.17 D and

was generally much smaller for small powers. Similar accuracy was obtained when cylindrical lenses were used instead of spherical lenses. The error should be considered an upper bound on the error of the wave-front sensor, since some of these discrepancies may be attributable to manufacturing errors in the trial lenses. As expected, all the Zernike terms corresponding to aberrations other than either defocus or astigmatism, depending on the type of trial lens used, were very close to zero. Though we have not explicitly assessed the accuracy with which the wave-front sensor measures higher-order aberrations other than defocus and astigmatism, this shows that the wave-front sensor does not introduce spurious higher-order aberrations that are not present in the wave aberration. Since higher-order aberrations displace the images on the CCD, much like defocus and astigmatism but simply in a different pattern, it is reasonable to expect that the sensor produces accurate measurement of these aberrations as well.

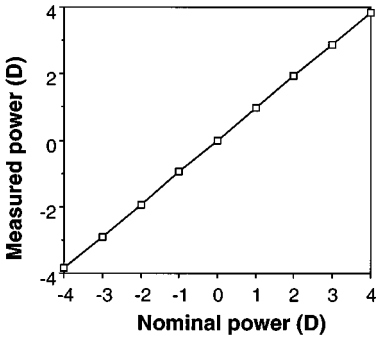

Fig. 5. Measurement of trial lenses with the wave-front sensor. The curve shows the power in diopters derived from the wave-front sensor as a function of the nominal power of trial lenses inserted into the system.

D. Comparison of the Wave-Front-Sensor MTF with Double-Pass and Interferometric Estimates of the Eye's MTF

In this section we compare estimates of the eye's MTF obtained with the wave-front sensor with results reported by Williams *et al.*[12] obtained with the double-pass and interferometric techniques. The wave-front-sensor measurements were carried out under conditions chosen to match those used in the double-pass and interferometric measurements. We used the same three observers, the same refractive state, the same alignment procedure, the same pupil size (3 mm), the same wavelength (632.8 nm), and the same retinal location (fovea). The wave-front-sensor measurements were made approximately 2 years after the interferometric and double-pass measurements.

Figures 6a.–c. show the MTF's of the three subjects obtained with the wave-front sensor compared with the MTF's obtained with the interferometric and double-pass techniques. The eye's MTF from the wave-front sensor was taken as the autocorrelation of the eye's pupil function. The MTF's from the wave-front sensor do not include the Stiles–Crawford effect. The Stiles–Crawford effect[15,16] is small at the foveal center,[17] and MTF's calculated for this pupil size (3 mm) incorporating the Stiles–Crawford effect were negligibly different from those calculated without it. Each MTF in Fig. 6 displays the cross section of the two-dimensional MTF corresponding to that for horizontal gratings. The double-pass technique produces the lowest MTF because of choroidal scatter, which grows in red light. Williams *et al.*[12] showed that when green light is used in the double-pass technique, the double-pass MTF was raised slightly into agreement with the interferometric MTF. This is probably because red

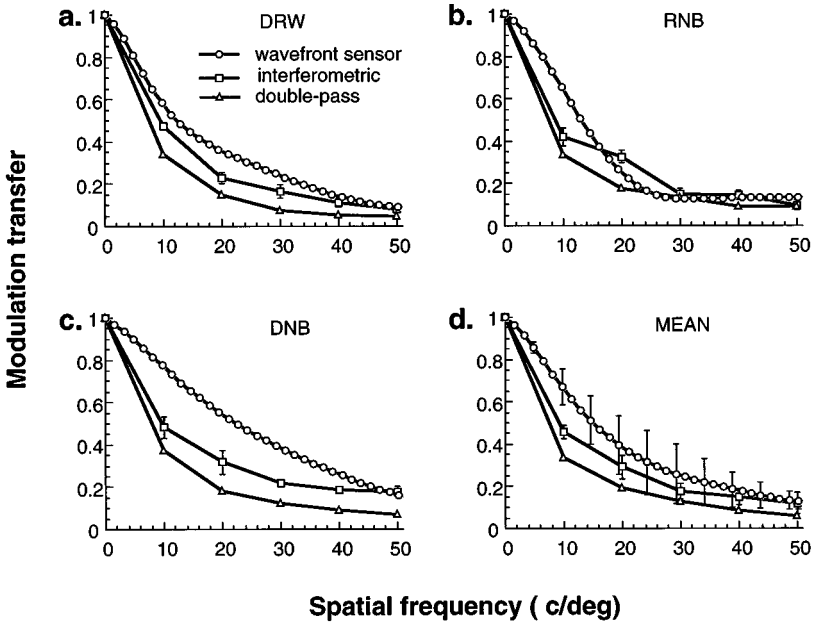

Fig. 6. Comparison of MTF's obtained with wave-front sensing, the double-pass method, and the interferometric technique. a.–c. compare the MTF's for each of the three observers, and d. shows the mean for the three observers. The interferometric and the double-pass data are from Williams *et al.*,[12] who studied the same observers measured here. The curves show the eye's MTF for horizontal gratings. The error bars for the interferometric MTF's are ±1 standard error of the measurements.

light is more subject to multiple scattering in the choroid than is green light.

The within-subject variability of the MTF obtained from wave-front sensing was very small; the standard error of the individual MTF's is smaller than the data points in Figs. 6a.–c. Nonetheless, as can be seen from the size of the error bars in Fig. 6d., the intersubject variability is greater for the wave-front-sensor MTF's than for either the double-pass or the interferometric MTF's. The wave-front-sensor data were collected in a single session on a single day, whereas the interferometric and double-pass methods involved measurements over several days. It is possible that day-to-day variation in the eye's MTF, perhaps as a result of shifts of refractive state and alignment, can explain this difference.

In all three subjects the MTF from the wave-front-sensor lies somewhat above the interferometric data at lower spatial frequencies but agrees well at the highest spatial frequencies. One hypothesis is that forward light scatter may account for the discrepancy. The wave-front sensor discretely samples the pupil and does not capture imperfections in the eye's optics at a very fine spatial scale such as those that would cause forward light scatter. To explain the low-frequency discrepancy, forward scatter would have to produce a relatively broad skirt in the eye's point-spread function that affected the interferometric and the double-pass but not the wave-front-sensor measurements. However, such a skirt would reduce modulation transfer at high as well as at low spatial frequencies, yet the discrepancy is confined to low frequencies. Therefore it does not appear that forward scatter by itself will explain the higher wave-front-sensor MTF's at low frequencies.

Another possibility is that the refractive state of the observers in the different experiments was different. Although the same grating target and procedure were used in each case, the wave-front-sensor data were collected within a single experimental session, whereas the interferometric data were obtained in several sessions each of greater length and were run on different days. It is conceivable that the refractive error was somewhat larger in the longer, interferometric experiments. The amount of defocus required to bring the mean MTF's into approximate register is only ~0.15 diopters. Another factor that could contribute to the discrepancy is differences in pupil alignment. Although the same subjective criterion, optimum image quality of a horizontal grating, was used for all three methods, we do not know whether the subjects selected the same pupil location with each method.

Despite these small differences among the MTF's obtained with different techniques, the three techniques yield reasonably similar MTF's. The Hartmann–Shack wave-front sensor captures the most important sources of image blur, a conclusion that is also supported by evidence that wave-front-sensor data can be used to correct higher-order aberrations in the eye.[18] Although wave-front-sensing methods are insensitive to light scatter caused by structures on a spatial scale in the pupil finer than that of the sampling array, the agreement in Fig. 6 shows that in the normal eye, light scatter is a minor source of image blur compared with the aberrations that the wave-front sensor can measure.

E. Comparison of the Wave-Front-Sensor MTF with the MTF from the Objective Aberroscope

Figure 7 compares the wave-front-sensor MTF with that from the aberroscope,[19] both for a 3-mm pupil. Defocus and astigmatism have been removed from the wave-front-sensor MTF's, as they were from the data of Walsh and Charman.[19] The wave-front sensor produces an MTF that lies below that of the aberroscope. This difference could be due to individual differences among the subjects in the two studies, which is known to be large.[3,4] To evaluate this possibility, we computed the MTF's from the 12 observers measured with the wave-front sensor for a 3.4-mm pupil. The shaded area in Fig. 7 indicates the range of MTF's obtained with the wave-front sensor, showing that the Walsh and Charman data lie at the upper edge of our sample. Walsh and Charman's MTF is for a wavelength of 590 rather than 633 nm, but we expect this difference to be relatively unimportant. Although it is true that short wavelengths will generally produce a higher MTF in an optical system that has no or little aberrations, the aberrations in real eyes tend to mask this effect. The reason is that a fixed wave aberration produces a larger reduction in the MTF for shorter wavelengths, roughly compensating for the reduced effect of diffraction.

Another possibility is that the difference is related to the finer spatial scale with which we analyzed the wave aberration. The wave-front sensor had a fourfold increase in pupil sampling density relative to the aberroscope, and the wave aberration was described with basis functions up to tenth order instead of only fourth order, which corresponds to a greater than fourfold increase in the number of modes characterized in each eye.

The 65 polynomials in the wave-front fit include all Zernike modes with radial power less than or equal to 10,

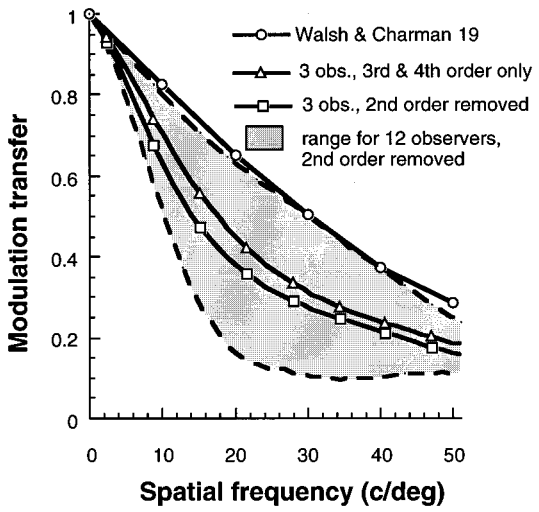

Fig. 7. Comparison of MTF's obtained with the wave-front sensor and with the aberroscope for a 3-mm pupil. Circles show the MTF of the eye from the objective aberroscope.[19] Squares show, for three observers, the mean MTF's with both defocus and astigmatism removed. Triangles show, for the same observers, the mean MTF's derived from wave aberrations that included only third- and fourth-order Zernike aberrations, with higher and lower orders removed. The shaded area shows the range of the MTF's for 12 eyes for a 3-mm pupil measured with our wave-front sensor.

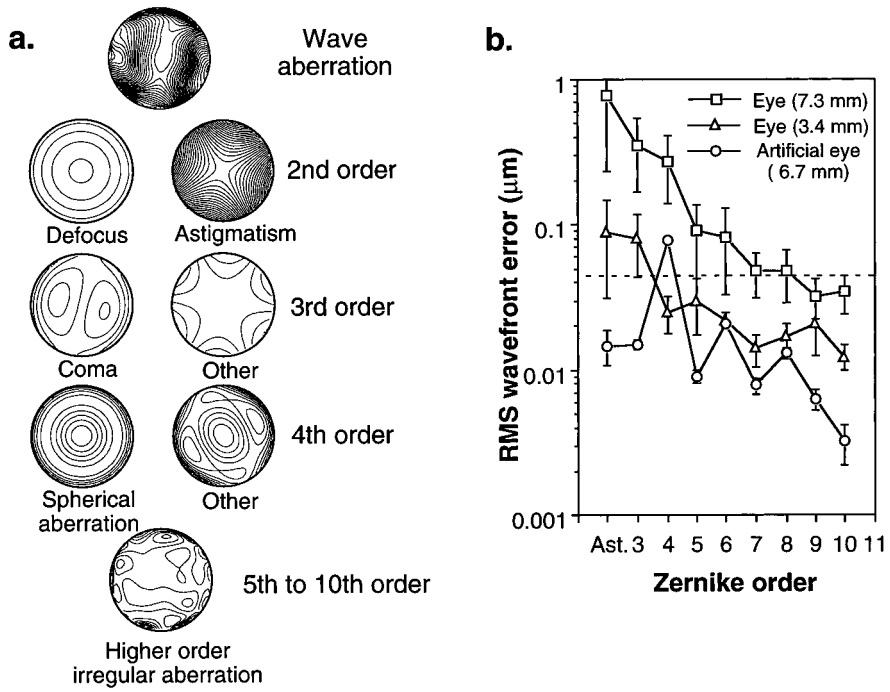

Fig. 8. Zernike description of the eye's aberrations. a. The wave aberration in YL's eye for a 7.3-mm pupil, shown at the top, is decomposed into Zernike polynomials up to tenth order. Contour line spacing is 0.15 μm. Modes shown include classical aberrations such as defocus (0.1 D), astigmatism (0.8 D at 15 deg), coma, and spherical aberration. The decomposition reveals higher-order, irregular aberrations in addition to classical aberrations. b. The upper curve (squares) shows the RMS wave-front error of each Zernike order for a 7.3-mm pupil averaged across 14 human eyes. Error bars indicate the standard deviation among eyes. For the second-order Zernike modes, only astigmatism is shown. The average amount of astigmatism in these observers was 0.6 D, corresponding to a mean RMS value of 0.77 μm. The middle curve (triangles) shows the data for a 3.4-mm pupil averaged across 12 tested eyes. The lower curve (circles) is for an artificial eye. The error bars show the standard deviation of ten repeated measurements.

except for the piston term. The first-order Zernike modes are the linear terms (corresponding to tilt, which we ignore here). The second-order modes are the quadratic terms corresponding to the familiar aberrations—defocus and astigmatism. The third-order modes represent coma and comalike aberrations. The fourth order contains spherical aberration as well as other modes. The fifth to tenth orders are the higher-order, irregular aberrations. Local irregularities in the wave front within the pupil are represented by these higher-order Zernike modes. For this pupil size, the wave-front-sensor data show that aberrations higher than fourth order play a very small role. The square symbols in Fig. 7 show the MTF for the original three observers when defocus and astigmatism have been corrected. The triangles show the MTF when the irregular aberrations corresponding to orders 5–10 have been removed, leaving only diffraction and third- and fourth-order aberrations to determine the MTF. There is little difference between these two MTF's, indicating that aberrations corresponding to orders 5–10 do not play an important role in image quality for 3-mm pupils.

F. Irregular Aberrations

Irregular aberrations play a more significant role when the pupil is large. In that case, the aberrations of the eye are not well described by the classic aberrations of conventional optical systems. Figure 8a. shows the Zernike decomposition of the wave aberration of subject LY's eye for a 7.3-mm pupil. The contribution of the classic aberrations such as defocus, astigmatism, coma, and spherical aberration, as well as irregular aberrations, are shown.

The root-mean-square (RMS) error of an individual Zernike order is a measure of that order's role in degrading optical quality. Figure 8b. shows the RMS wave-front error contributed by each Zernike order for a 3.4-mm pupil (triangles), a 7.3-mm pupil (squares), and an artificial eye with a 6.7-mm pupil (circles). The average RMS wave-front error decreases monotonically as the Zernike order increases for both pupil sizes in the human eye, though the pattern varies somewhat among individual observers. The RMS error for the small pupil lies 3–4 times lower than that for the large pupil of real eyes. This illustrates the well-known fact that aberrations grow with increasing pupil size. An RMS error of $\lambda/14$ (0.045 μm at 0.633 μm) is a common tolerance for diffraction-limited performance in an optical system.[14] For the 3.4-mm pupil, only Zernike orders up to third order exceed this tolerance. At the larger pupil size, however, the mean RMS value of each Zernike order from 2 to 8 is greater than $\lambda/14$.

Figure 8b. also shows the RMS wave-front error for an artificial eye (circles) measured with the same instrument. The artificial eye consisted of an achromatic dou-

blet (f = 16 mm) and a diffuser to mimic the retina. Though our measurements reveal some expected spherical aberration in the artificial eye, the mean RMS value of each order averages approximately one order of magnitude lower than in human eyes for the large (7.3-mm) pupil. This indicates that the measured higher-order, irregular aberrations are true defects of the human eyes and not aberrations in the apparatus.

G. Similarity of Left and Right Eyes

We confirmed previous reports[3,4] that aberrations differ greatly from observer to observer. This leads to the speculation that aberrations in the eye may not be systematic but rather reflect random errors in the structure of the lens and cornea. However, we found that aberrations are relatively similar between the left and right eyes of the same observer. This can be seen in Fig. 9a. which shows three-dimensional plots of the wave aberrations of two observers. Figure 9b. shows the Zernike coefficients of the left eye plotted against the same coefficient of the right eye. The data points lie close to a straight line, with a slope of 1 indicating the correlation between the aberrations of the left and right eyes.

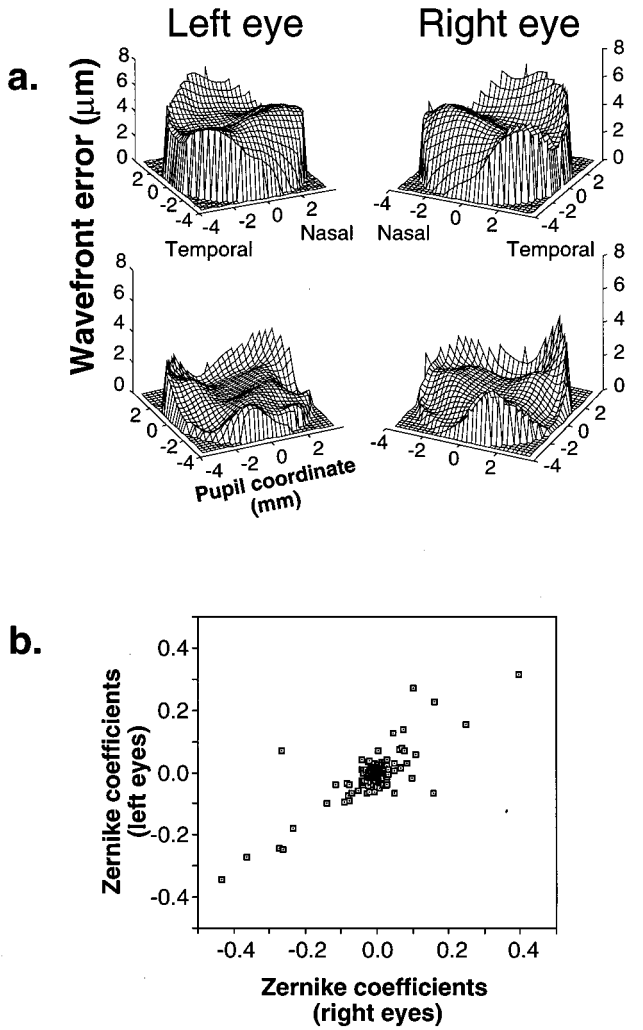

Fig. 9. Similarity of the eye's aberrations in the left and right eyes. a. Three-dimensional surface plots of the wave aberration of the left and right eyes of two observers, showing the mirror symmetry of left and right eyes. Defocus and astigmatism have been removed from the wave aberration. b. Coefficients of individual Zernike modes in the right eye plotted against the corresponding coefficients of the left eye, showing the correlation between left and right eyes. Data of four subjects are combined.

H. Modulation Transfer Functions and Pupil Size

From our measurements of the eye's wave aberration for a small (3.4-mm) and a large (7.3-mm) pupil, we show in Fig. 10 the mean MTF for pupil sizes from 2 to 7.3 mm. The eye's MTF's were computed from the wave aberration, assuming uniform transmittance across the pupil.[20,21] Our results are in qualitative agreement with those from other methods such as the interferometric technique[22] and the double-pass technique,[23] and from measurements of the eye's wave aberration.[24] Specifically, at low frequencies the MTF is highest for pupils between 2 and 3 mm, with aberrations reducing modulation transfer for larger pupils. At high frequencies as shown in Fig. 10b., however, larger pupil sizes provide improved modulation transfer despite the presence of aberrations.

I. Influence of the Higher-Order Irregular Aberrations on the Eye's MTF for Small and Large Pupils

In this section we show the importance of higher-order aberrations for retinal image quality. Figure 11a. shows the MTF (squares) when only defocus and astigmatism have been corrected for the 3-mm pupil. This curve lies well below the uppermost curve, which is the MTF for an aberration-free 3-mm pupil. This discrepancy shows the degradation of the eye's optical quality by the eye's monochromatic aberrations. Triangular symbols show the MTF if second-, third-, and fourth-order aberrations were corrected, leaving only the higher-order, irregular aberrations to produce image blur. There is little difference between this curve and diffraction alone. As the upper curves in Fig. 11a. show, the ratio of the diffraction MTF to the MTF with only defocus and astigmatism corrected grows to more than a factor of 2 at high spatial frequencies. The higher-order (fifth–tenth) irregular aberrations by themselves reduce image contrast by less than 30%.

In contrast, Fig. 11b. shows the MTF (squares) when only defocus and astigmatism have been corrected for the 7.3-mm pupil. This curve lies far below the uppermost curve, which is the MTF for an aberration-free 7.3-mm pupil. This discrepancy reveals the deleterious effect of the eye's monochromatic aberrations on retinal image quality. Triangles show the MTF if second-, third-, and fourth-order aberrations were corrected. Even in this case, the higher-order, irregular aberrations produce a substantial loss in retinal image quality compared with an eye suffering only from diffraction. As shown by the upper curves, the ratio of the diffraction MTF to the MTF with only defocus and astigmatism corrected grows to more than a factor of 10 at high spatial frequencies. Even the higher-order (fifth–tenth) irregular aberrations by themselves reduce image contrast by up to three to four times at high frequencies.

J. Strehl Ratio and Higher-Order Aberrations

One important reason to characterize higher-order aberrations is to determine how much improvement in retinal

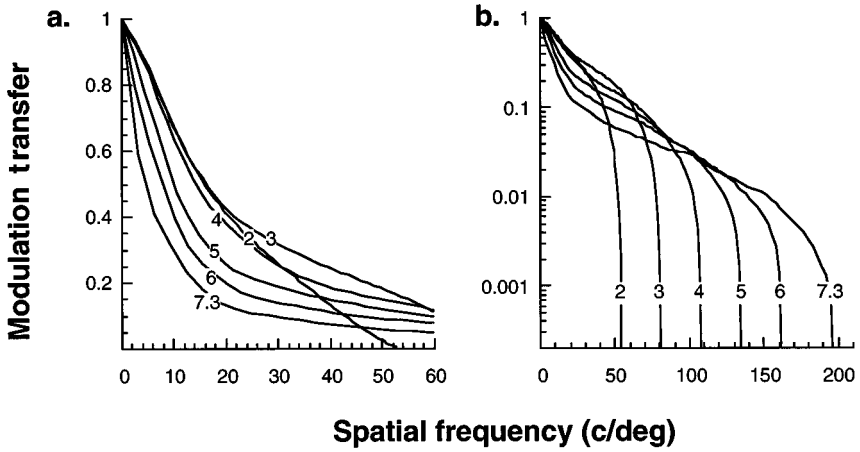

Fig. 10. Mean of the radially averaged MTF's of the eye for different pupil sizes. The numbers on the curves indicate the pupil size of the eye. The mean MTF's for a 2- and a 3-mm pupil are derived from the wave aberration of 12 eyes measured across a 3.4-mm pupil, and the mean MTF's for 4-, 5-, 6-, and 7.3-mm pupils are derived from the wave aberration of 14 eyes measured across a 7.3-mm pupil. Defocus and astigmatism were removed for each eye and each pupil size. Plots a. (linear) and b. (semilog) are from the same data.

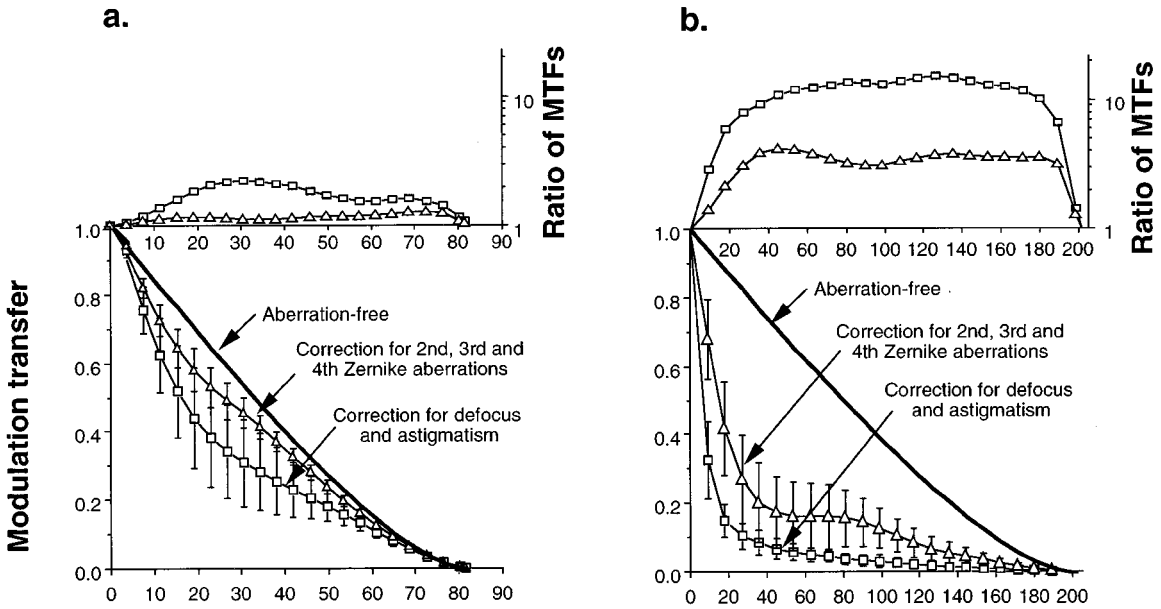

Fig. 11. Mean of the radially averaged MTF's for two pupil sizes: a. 3 mm and b. 7.3 mm. The top curve in the lower part of the figure is the MTF for an aberration-free eye, in which diffraction is the sole source of image blur. The lowest curve is for eyes corrected to remove defocus and astigmatism entirely. The middle curve is for eyes with second-, third-, and fourth-order Zernike aberrations corrected but with the higher-order, irregular aberrations (orders 5–10) uncorrected. The error bars are the standard deviation of 12 tested eyes for the small (3-mm) pupil and of 14 tested eyes for the large (7.3-mm) pupil. The upper part of the figure plots the ratio of the diffraction MTF to the mean MTF of real eyes if only defocus and astigmatism are corrected (squares) and the ratio of the diffraction MTF to the mean MTF of real eyes if the higher-order (fifth to tenth) irregular aberrations remain uncorrected (triangles).

image quality could be achieved by correcting various aberrations. For this purpose we use the Strehl ratio as a metric for retinal image quality. The Strehl ratio, which can range from 0 to 1, is the ratio of the peak intensity of the eye's PSF to that of a PSF for an aberration-free eye with the same pupil size, in which diffraction is the only source of blur. Strehl ratios greater than 0.8 are generally considered to correspond to diffraction-limited imaging.[14]

Figure 12 shows how the Strehl ratio for 3- and 7.3-mm pupils improves as we remove successively higher Zernike orders from the wave aberration. For example, the value of 4 in the abscissa corresponds to the case in which the second-, third-, and fourth-order Zernike aberrations have been removed from the wave aberration. One can think of the removal of Zernike orders as corresponding to the effect of a hypothetical optical element akin to a deformable mirror that was capable of correcting lower-order aberrations while leaving the higher-order aberrations unaffected. For 3-mm pupils, one need correct only second-, third-, and fourth-order aberrations to achieve a diffraction-limited Strehl ratio. However, for 7.3-mm pupils, Zernike orders up to and including at least eighth order must be corrected to achieve diffraction-limited per-

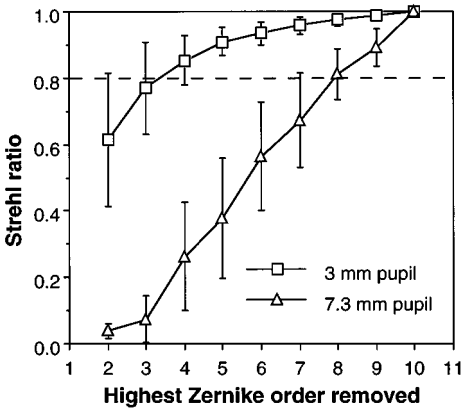

Fig. 12. Strehl ratio of the eye's PSF for a 3-mm pupil (squares) and for a 7.3-mm pupil (triangles). Error bars show the standard deviation of 12 tested eyes for the 3-mm pupil and of 14 tested eyes for the 7.3-mm pupil. Each data point shows the Strehl ratio that would have been obtained with lower Zernike orders removed to provide a measure of optical quality were lower orders corrected. The abscissa indicates the highest lower order removed in each case. For example, a value of 2 on the abscissa means that only second-order aberrations, corresponding to defocus and astigmatism, have been removed. A value of 3 indicates that both second- and third-order aberrations have been removed.

formance. This should be considered a lower bound because it assumes that all the eye's aberrations are described with a tenth-order fit. Although the trend illustrated in Fig. 8 would suggest that still-higher-order aberrations than tenth are relatively unimportant, they presumably also reduce retinal image quality to some extent.

4. DISCUSSION

Unlike other techniques that measure only the eye's MTF[12,22,23,25–27] techniques such as the aberroscopic method and wave-front sensing also measure the phase transfer function of the eye, which plays an important role in retinal image quality when the pupil is large.[28] In addition, these techniques measure the wave aberration simultaneously at many locations throughout the pupil, unlike psychophysical methods,[7,29,2,30] which must sequentially map the pupil point by point. Rapid measurement can reduce the possibility that temporal fluctuations of refractive state will distort the estimate of the wave aberration. The knife-edge technique[6] allows simultaneous measurement of the entire pupil, but the phase error at each location is estimated from the intensity of the light at each point of the pupil, which can be confounded with other factors such as the Stiles–Crawford effect. The wave-front sensor's measurements are independent of intensity variations in the light returning from the retina.

The objective aberroscope[4] provides simultaneous wave-aberration measurements of the entire pupil but cannot sample the pupil with a spacing finer than ~0.9 mm.[31] Our wave-front sensor shows that it is possible to sample the pupil at a much finer spatial scale. For example, for the 3.4-mm pupil measurements, a sample spacing of 0.2 mm was used, which is more than four times smaller. In principle, even finer sampling could be employed. Finer sampling helps to characterize the more abrupt changes in phase error associated with irregular aberrations. A preliminary comparison of the wave aberration obtained with fine (0.2 mm) and coarse (0.42 mm) sampling for the same pupil size suggested that the finer sampling produced somewhat higher estimates of the eye's aberrations. Our wave-front sensor has a number of potential applications because of its ability to reliably capture irregularities at small as well as large spatial scales in the pupil. Because the PSF of the eye (or alternatively the MTF and the phase transfer function) can be computed from the wave aberration, wave-front sensing reveals the impact of these irregularities on retinal image quality. Conventional measures of visual performance, such as Snellen acuity or contrast sensitivity, do not link visual performance to specific defects in the eye's optics. Wave-front sensing can be used to measure the wave aberration before and after laser refractive surgery,[32,33] to quantitatively describe the optical consequences of corneal ablation and perhaps ultimately to provide a superior visual outcome. Moreover, it can aid in the design and fitting of contact lenses, so that one could develop techniques to correct additional aberrations besides defocus and astigmatism. The wave-front sensor can also be used in conjunction with a deformable mirror to compensate for the eye's wave aberration, providing supernormal vision and unprecedented resolution for retinal imaging.[18]

Although it is well known that defocus and astigmatism tend to be correlated in left and right eyes, we find that this principle can be extended to other aberrations as well. The genetic and environmental factors that control all the aberrations of the eye's dioptrics must operate in approximate mirror symmetry on the left and right eyes.

The biological optics of the human eye reveal local irregularities that are not present in man-made optics. The wave-front measurements provide the most complete description of the eye's aberrations, showing conclusively that for large pupils the eye suffers from higher-order, irregular aberrations. These irregular aberrations do not reduce visual performance when the pupil is small (~3 mm), such as in very-high-light-level conditions. However, they do reduce retinal image contrast in the visible range of spatial frequencies when the pupil is large. For example, for a 7.3-mm pupil at 20 c/deg, aberrations beyond defocus and astigmatism reduce retinal image contrast by a factor of approximately 7. The effect of these aberrations is especially deleterious in attempts to image the retina at very high resolution.[34] To obtain diffraction-limited retinal imaging with large pupils, methods such as adaptive optics must correct these irregular aberrations as well as the classical, lower-order defects in the eye.

ACKNOWLEDGMENTS

This research is supported by National Institutes of Health grants EY04367 and EY01319, a Rochester Eye and Human Parts Bank fellowship, and an ophthalmology development grant from Research to Prevent Blindness, Inc. The authors thank Don Miller and G. Michael Morris for their contributions to this work.

REFERENCES AND NOTES

1. W. M. Rosenblum and J. L. Christensen, "Objective and subjective spherical aberration measurement of the human eye," in *Progress in Optics*, E. Wolf, ed. (North-Holland, Amsterdam, 1976), Vol. 13, pp. 69–91.
2. M. C. Campbell, E. M. Harrison, and P. Simonet, "Psychophysical measurement of the blur on the retina due to optical aberrations of the eye," Vision Res. **30**, 1587–1602 (1990).
3. H. C. Howland and B. Howland, "A subjective method for the measurement of monochromatic aberrations of the eye," J. Opt. Soc. Am. **67**, 1508–1518 (1977).
4. G. Walsh, W. N. Charman, and H. C. Howland, "Objective technique for the determination of monochromatic aberrations of the human eye," J. Opt. Soc. Am. A **1**, 987–992 (1984).
5. H. von Helmholtz, *Physiological Optics*, J. P. C. Southall, ed. (Dover, New York, 1896).
6. F. Berny, S. Slansky, "Wavefront determination resulting from foucault test as applied to the human eye and visual instruments," in *Optical Instruments and Techniques*, J. H. Dickenson, ed. (Oriel, Newcastle, UK, 1969), pp. 375–386.
7. G. Van den Brink, "Measurements of the geometrical aberrations of the eye," Vision Res. **2**, 233–244 (1962).
8. H. C. Howland and J. Buettner, "Computing high order wave aberration coefficients from variations of best focus for small artificial pupils," Vision Res. **29**, 979–983 (1989).
9. J. Liang, B. Grimm, S. Goelz, and J. Bille, "Objective measurement of the wave aberrations of the human eye with the use of a Hartmann–Shack wave-front sensor," J. Opt. Soc. Am. A **11**, 1949–1957 (1994).
10. B. Platt and R. V. Shack, "Lenticular Hartmann screen," Opt. Sci. Center Newsl. (University of Arizona) **5**, 15–16 (1971).
11. D. H. Sliney and M. L. Wolbarsht, "Safety standards and measurement techniques for high intensity light sources," Vision Res. **20**, 1133–1142 (1980).
12. D. R. Williams, D. H. Brainard, M. J. McMahon, and R. Navarro, "Double-pass and interferometric measures of the optical quality of the eye," J. Opt. Soc. Am. A **11**, 3123–3135 (1994).
13. W. H. Southwell, "Wave-front estimation from wave-front slope measurements," J. Opt. Soc. Am. A **70**, 998–1006 (1980).
14. M. Born and E. Wolf, *Principles of Optics* (Pergamon, Oxford, 1983).
15. W. S. Stiles and B. H. Crawford, "The luminous efficiency of rays entering the eye pupil at different points," Proc. R. Soc. London Ser. B **112**, 428–450 (1933).
16. J. Enoch and V. Lakshminarayanan, "Retinal fibre optics," in *Visual Optics and Instrumentation*, W. N. Charman, ed., Vol. 1 of Vision and Visual Dysfunction, J. Cronly-Dillon, ed. (CRC, Boca Raton, Fla., 1991), Chap. 12.
17. G. Westheimer, "Dependence of the magnitude of the Stiles–Crawford effect on retinal location," J. Physiol. (London) **192**, 309–315 (1967).
18. J. Liang, D. R. Williams, and D. T. Miller, "Supernormal vision and high-resolution retinal imaging through adaptive optics," J. Opt. Soc. Am. A **14**, 2884–2892 (1997).
19. G. Walsh and W. N. Charman, "The effect of pupil centration and diameter on ocular performance," Vision Res. **28**, 659–665 (1988).
20. J. W. Goodman, *Introduction to Fourier Optics* (McGraw-Hill, San Francisco, Calif., 1968).
21. We have also calculated the eye's MTF, incorporating the Stiles–Crawford effect ($\rho = 0.05$). The MTF is increased slightly at lower frequencies but is reduced at higher frequencies; nevertheless, the Stiles–Crawford effect does not substantially change our conclusions.
22. F. W. Campbell and D. G. Green, "Optical and retinal factors affecting visual resolution," J. Physiol. (London) **181**, 576–593 (1965).
23. F. W. Campbell and R. W. Gubisch, "Optical quality of the human eye," J. Physiol. (London) **186**, 558–578 (1966).
24. G. Walsh and W. N. Charman, "Measurement of the axial wavefront aberration of the human eye," Ophthalmic. Physiol. Opt. **5**, 23–31 (1985).
25. F. Flamant, "Etude de la repartition de lumière dans l'image rétinienne d'une fente," Rev. Opt. Theor. Instrum. **34**, 433–459 (1955).
26. G. Westheimer and F. W. Campbell, "Light distribution in the image formed by the living human eye," J. Opt. Soc. Am. **52**, 1040–1044 (1962).
27. P. Artal, S. Marcos, R. Navarro, and D. R. Williams, "Odd aberrations and double-pass measurements of retinal image quality," J. Opt. Soc. Am. A **12**, 195–201 (1995).
28. W. N. Charman and G. Walsh, "The optical phase transfer function of the eye and the perception of spatial phase," Vision Res. **25**, 619–623 (1985).
29. M. S. Smirnov, "Measurement of the wave aberration of the human eye," Biophys. J. **7**, 766–795 (1962).
30. R. H. Webb, C. M. Penney, and K. P. Thompson, "Measurement of ocular wave-front distortion with a spatially resolved refractometer," Appl. Opt. **31**, 3678–3686 (1992).
31. W. N. Charman, "Wave aberration of the eye: a review," Optom. Vis. Sci. **68**, 574–583 (1991).
32. R. A. Applegate, C. A. Johnson, H. C. Howland, and R. W. Yee, "Monochromatic wavefront aberrations following radial keratotomy," in *Noninvasive Assessment of Visual System*, Vol. 7 of 1989 OSA Technical Digest Series (Optical Society of America, Washington, D.C., 1989), pp. 98–102.
33. R. A. Applegate and K. A. Gansel, "The importance of pupil size in optical quality measurements following radial keratotomy," Refract. Corneal Surg. **6**, 47–54 (1990).
34. D. T. Miller, D. R. Williams, G. M. Morris, and J. Liang, "Images of the cone mosaic in the living human eye," Vision Res. **36**, 1067–1079 (1996).